technical memorandum Daresbury Laboratory

DL/SCI/TM40E

MULTIWIRE PROPORTIONAL DETECTORS FOR USE IN A SMALL ANGLE SCATTERING EXPERIMENT: SOME DESIGN CONSIDERATIONS

by

J. STEIJGER, Netherlands Organisation for the Advancement of Pure Research (ZWO) and Daresbury Laboratory.

SEPTEMBER, 1984

Science & Engineering Research Council

Daresbury Laboratory

Daresbury, Warrington WA4 4AD

MULTIWIRE PROPORTIONAL DETECTORS FOR USE IN A SMALL ANGLE SCATTERING EXPERIMENT: SOME DESIGN CONSIDERATIONS

J. STEIJGER

Netherlands Organisation for the Advancement of Pure Research (ZWO)

and

Science and Engineering Research Council, Daresbury Laboratory,

Daresbury, Warrington WA4 4AD, U.K.

SCIENCE AND ENGINEERING RESEARCH COUNCIL

DARESBURY LABORATORY

Contents

1. Introduction

Since Charpak [1] constructed the first MultiWire Proportional Chamber (MWPC), and operated the device successfully, more than a decade and a half elapsed in which numerous workers have published their experiences with MWPC's. High energy physicists rank amongst the first and most frequent users, but the devices have also been used for the detection of X-rays. This latter application, particularly the high counting-rate capability, is of considerable interest in Small Angle Scattering (SAS) experiments.

In the design stage of a small angle scattering workstation at the Synchrotron Radiation Source at Daresbury, a short review was needed on the detection-, electrical-, and mechanical properties of the MWPC as a fast linear position-sensitive detector of X-rays with energies near 8 keV. Although a very good review by Sauli [2] is already available, the author felt it not unprofitable to write this report which serves a different purpose and includes more recent literature.

In the following sections a typical MWPC will be described, its design parameters identified and the most important features of the electrostatic field given (section 2). Section 3 deals with the mechanical properties of the chamber, and includes a discussion of the mechanical tolerances and their effects on the gas amplification in particular. Section 4 gives some data on the absorption of 8 keV photons in the gas and in window materials. The effects of the preamplifier on the pulses from the wires of the chamber is the subject of section 5, and, finally, section 6 gives some ideas on the resolution which can be obtained with these devices.

2. Electrostatic properties

It was recognised by Charpak and co-workers [1] that several anode-wires stretched parallel to each other in the same volume of gas and at the same potential, act as a set of independent counters. Figure 1 shows a cross-section through a plane perpendicular to the anode wires, and defines a coordinate system as follows. The wires run along the z-direction and are stretched in the xz-plane a distance 's', the pitch, apart. Two cathode planes are placed a distance 'a' away from and parallel to the xz-plane, in which the anode wires lie. The diameter of the wires is d and their length is ℓ. SI-units are used throughout this report. In the following the properties of a few chambers, which have values for a, s, and d of interest for our application, are compared. The formulae will be given for general a, s, and d values.

The electrostatic properties of an electrode system which extends infinitely in the x- and z-directions has been given by Erskine [3], from which work the following expressions are taken. The differences in the formulae presented here, and those found in ref.3 are solely attributable to the use of different units. When a potential difference is applied to the cathode planes and anode wires an electric field will develop, and a charge will be gathered on the electrodes. Erskine started from the expression of the potential

$$V(x,y) = \frac{q}{4\pi\epsilon_0}\left\{\frac{2\pi a}{s} - \ell n[4(\sin^2(\pi x/s) + \sinh^2(\pi y/s))]\right\} \qquad (2.1)$$

where $4\pi\epsilon_0 = 1.11 \times 10^{-10}$ F/m, and q the charge on a unit length of an anode wire. This expression satisfies the conditions $V(x,\pm a) = 0$ and $V(ns\pm d/2,0) = V_0$ = the applied potential difference, approximately. The

charge per unit length on the anode wires may be solved from

$V(d/2,0) = V_0$ obtaining

$$q = \frac{2\pi\varepsilon_0 V_0}{\pi a/s - \ell n(\pi d/s)} \qquad (2.2)$$

The capacitance per unit length of the anode wire may be found by setting $c = q/V_0$, and is included for easy reference

$$c = \frac{2\pi\varepsilon_0}{\pi a/s - \ell n(\pi d/s)} \qquad (2.3)$$

The electric fieldstrength can be determined by taking

$\vec{E}(x,y) = -\vec{\nabla} V(x,y)$ with the result

$$E_x(x,y) = \frac{q}{2\varepsilon_0 s} \frac{\sin(\pi x/s)\cos(\pi x/s)}{\sin^2(\pi x/s) + \sinh^2(\pi y/s)} \qquad (2.4a)$$

$$E_y(x,y) = \frac{q}{2\varepsilon_0 s} \frac{\sinh(\pi y/s)\cosh(\pi y/s)}{\sin^2(\pi x/s) + \sinh^2(\pi y/s)} \qquad (2.4b)$$

Three regions of interest may now be identified. Firstly the field region a distance more than about s above and below the anode wire plane. In this case $\sinh^2(\pi y/s)$ is greater than 133 and becoming larger rapidly with increasing distance. Moreover, $\sinh(\pi y/s)$ becomes more and more nearly equal to $\cosh(\pi y/s)$, so that in this region $E_x(x,y \gtrsim s) \approx 0$ and $E_y(x,y \gtrsim s) \approx q/2\varepsilon_0 s$. Therefore, we observe that this region is characterized by a homogeneous electric field. Table 1 shows the maximum deviations from uniformity for a number of distances y from the anode plane. The second region of interest is close to a wire, i.e. small values for both x and y. In this case the following approximations are valid

$\sin u \approx u - 1/6\ u^3 + \ldots$

$\sinh u \approx u + 1/6\ u^3 + \ldots$

and the electric field in this region may be written as:
$\vec{E}(\vec{R}) = (q/2\pi\varepsilon_0)\vec{R}/|\vec{R}|^2$, where $\vec{R}$ is the vector from a wire to the point of interest. This approximation is valid to the fourth order in $\pi|\vec{R}|/s$, so for $|\vec{R}| < 0.1s$ the error is certainly less than 1 percent. Finally, the third region of interest is within the $y \approx 0$ plane, but between wires. In this region $\sinh(\pi y/s)$ is very small, $\cosh(\pi y/s)$ very nearly equal to 1, as is $\sin(\pi x/s)$. $\cos(\pi x/s)$, finally, may be approximated by $\pi x/s$ in this region. Both E_x and E_y appear then to be small.

In summary, one observes in a MWPC the presence of three different regions in the electric field: a uniform field is present in the region given by $|y| \gtrsim s$, and any x and z, secondly a high radial field region is present around the wires, and lastly a low field region in between wires. This, and the relevant expressions for the electric fieldstrength, are given in table 2.

Following Beingessner [4] we also may calculate the field near the cathode as follows. From electrostatic theory $E = \sigma/\varepsilon_0$, where E is the electric fieldstrength directed normally to a conductor which carries a charge per unit area equal to σ. Assuming the total charge on the chamber to be zero, each cathode plane carries a charge

$$\sigma = q/2s \qquad (2.5)$$

giving rise to an electric field equal to

$$E = q/2\varepsilon_0 s, \qquad (2.6)$$

which is the same expression as that given in table 2. However, with this formula we may also derive the field near a wire cathode plane. When the cathode plane is replaced by a wire plane, each wire having a diameter of d_c and stretched at a pitch s_c, the charge per unit area of conductor becomes

$$\sigma = q\, s_c/(\pi s_a d_c) \qquad (2.7)$$

from which the electric fieldstrength follows

$$E = q\, s_c/(\varepsilon_0 \pi s_a d_c) \qquad (2.8)$$

This field is, except in the case where the cathode wires nearly touch each other, stronger than that on a foil. For reasons to be discussed later, this means that a wire plane cathode gives rise more rapidly to instabilities in the chamber.

Since a detailed description of the physical principles of this detector is beyond the scope of this report, it suffices to give a few expressions which determine approximately the gas amplification in the device. This gas amplification occurs in the high radial field region, very near to the anode wire, and so depends on the electric field, and the properties of the gas in that region. The important parameters are thus immediately identified: d and q determine the field around the wire, the pressure p of the gas determines the number of gas molecules available for ionization, and a few constants determined by the nature of the

gas mixture, are necessary to describe these ionization properties. For our applications, however, operation is well into the proportional amplification region, and a fairly simple empiric formula applies:

$$A = \text{constant} \times \exp([q]) \qquad (2.9)$$

or:

$$A = \text{constant} \times \exp([E_0 . d]) \qquad (2.10)$$

In these expressions the square brackets denote the numerical value of the expression enclosed; E_0 is the field on the anode wire, and the constant is a function of the nature of the gas and a homogeneously decreasing function of the pressure. Although this constant may take wildly different values for different gas mixtures, it appears after an evaluation of 14 recently reported devices (see table 3) that the value of q rather than that of A is a constant. The devices selected for this table are all used for the detection of low energy X-rays with or without some measure of energy resolution i.e. at the highest gas amplifications practicable. Since this table reflects the experience of the authors, it may be used to fix a relation between the design-parameters a, s, d, and V_0.

3. Mechanical properties

In this section we will discuss three main topics. Firstly the forces on the signal wire plane, secondly the forces on the cathode foils, which may or may not be used as a window, and finally the electrical (in)stability of the chamber as a result of mechanical tolerances.

3.1 Forces on the anode wires

Consider two infinitely long, parallel wires which carry a charge per unit length equal to q. The force on a length $d\ell$ of wire is then given by (see fig.2)

$$F_v = \int_{-\pi/2}^{\pi/2} (q\, q_\alpha / 4\pi\varepsilon_0 r_\alpha^2) \cos\alpha \, d\alpha \qquad (3.1)$$

where F_v is the force in the vertical direction, q the charge on a length $d\ell$, q_α the charge on a length $d\ell_\alpha$, r_α the distance between the two lengths of wire, and $d\ell_\alpha$ as indicated in the figure. The horizontal components of the force cancel since $\sin\alpha$ is an odd function of α. The force per unit length of the wires is then given by

$$F = F_v = 2q^2/4\pi\varepsilon_0 s \qquad (3.2)$$

where s is the distance between the wires.

We may now apply this result to calculate the forces on the anode wires. Since we assume the same tension to be applied to each wire, and the wires exert repulsive forces on each other as a result of the charge gathered on them, a configuration like that in fig.3 results. The force on an anode wire, numbered 0, originates from the odd numbered wires and is given by

$$F = \sum_{i=\pm1,\pm3,\ldots} \frac{2q^2}{(is)^2 + 4\delta^2} \cdot \frac{2\delta}{4\pi\varepsilon_0} \qquad (3.3)$$

where 2δ is the distance between the two wire planes, and F is again the force per unit length. For small δ the $4\delta^2$ in the denumerator of eq.(3.3) may be neglected, and the sum evaluated to obtain

$$F = \pi q^2 \delta / 4 s^2 \varepsilon_0 \, . \qquad (3.4)$$

The force on a wire in an actual chamber is smaller than given by this expression, since only a finite sum has to be calculated. Table 4 contains some values for F, and compares these with the gravity forces acting upon the wires when the anode wires are stretched horizontally. From these observations one may conclude immediately that a restoring force must be present with a force constant greater than $\pi q^2/4s^2\varepsilon_0$ in order to obtain a stable system, and that gravity becomes comparable to the electrostatic forces only if the deflection is of the order of a few μm.

The restoring force, which drives the wire back to its central position, is supplied partly by the tension induced by the slight elongation which occurs when the wire is displaced in the middle, and partly by the tension introduced in the construction of the chamber. Assuming that the curve which is followed by the wire does not deviate much from the straight line, and thus that the first derivatives of this curve are small, the restoring force is given by the expression:

$$F = - T \frac{\partial^2 y}{\partial z^2} \qquad (3.5)$$

and directed (approximately) perpendicular to the wire, i.e. in the y-direction. T in eq.(3.5) is the tension introduced in the wire, and F the restoring force per unit length. Equating expressions (3.4) and (3.5) gives the curve followed by the wire:

$$- T \frac{\partial^2 y}{\partial z^2} = \pi q^2 y / 4\varepsilon_0 s^2 \qquad (3.6)$$

Eq.(3.6) may be solved with the boundary conditions $y(0) = 0$ and $y(\ell) = 0$, imposed by the construction. The solution of (3.6) reads

$$y(z) = \delta \sin\left(\left(\frac{\pi q^2}{4\varepsilon_0 s^2 T}\right)^{1/2} z + \phi\right) \qquad (3.7)$$

From $y(0)$ follows: $\phi = 0$, and from $y(\ell) = 0$ may be inferred

$$\left(\frac{\pi q^2 \ell^2}{4\varepsilon_0 s^2 T}\right)^{1/2} = n\pi \qquad (3.8)$$

Eq.(3.8) tells us that the amplitude of the deflection δ will become so large that the total tension, i.e. the tension applied during construction plus the tension due to the elongation of the wire, will become equal to:

$$T = \frac{q^2 \ell^2}{4\pi\varepsilon_0 s^2 n^2} \qquad (3.9)$$

Where the applied tension is already larger than $q^2\ell^2/4\pi\varepsilon_0 s^2$, no solution with $\delta \neq 0$ is possible. Therefore, the criterion for stability in the position of the wires reads

$$T > \frac{q^2 \ell^2}{4\pi\varepsilon_0 s^2} \approx 2.25 \times 10^{-6} (\ell/s)^2 \ [N] \qquad (3.10)$$

In eq.(3.10) we made use of the observation in table 3 that $q \approx 1.58 \times 10^{-8}$ C/m. It does not contain the elastic modulus since for

tensions above this limit no deflections are involved.

If the chamber is operated in a horizontal orientation, the effect of gravity must be included in eq.(3.6). Gravity contributes, per unit length, the force

$$F_g = \rho S g \qquad (3.11)$$

where ρ is the density of the wire, S the area of cross-section and g the acceleration due to gravity. The new equation reads

$$- T \frac{\partial^2 y}{\partial z^2} = \pi q^2 y / 4\varepsilon_0 s^2 + \rho S g \qquad (3.12)$$

and has a similar solution to that of eq.(3.6). For tensions greater than given by eq.(3.10) a minimum deflection is found, but it is non-zero. The curve followed by the wire is given by

$$y = \frac{\rho S g \ 4\varepsilon_0 s^2}{\pi q^2} \left[\frac{\sin(uz) - \sin(u(z-\ell))}{\sin(u\ell)} - 1\right] \qquad (3.13)$$

where

$$u = \left(\frac{\pi q^2}{4\varepsilon_0 s^2 T}\right)^{1/2}.$$

The maximum deflection occurs at $z = \ell/2$, and amounts to (taking $q = 1.58 \times 10^{-8}$ C/m, $\rho = 19.3 \times 10^3$ kg/m^3 (for W), $g = 9.8$ m/s^2, and $\varepsilon_0 = 8.85$ pF/m)

$$\delta = 6.71 \times 10^9 \ d^2 \ s^2 \left[\left\{\cos(2.35 \times 10^{-3} \sqrt{1/T}\ \ell/s)\right\}^{-1} - 1\right] \qquad (3.14)$$

where d is again the diameter of the wire. For a typical MWPC this deflection is only very small, e.g. for s = 1 mm, ℓ = 100 mm, d = 10 μm and T = 0.1 N then δ = 0.24 μm.

Finally, we consider the situation that during construction, one of the wires is displaced out of the plane. The electrostatic force is uniform over its length in this case, and thus the system is basically the same as the one previously discussed, where a gravity field was present. The critical tension is therefore given by eq.(3.10), and the curve which is followed by the wire by eq.(3.13) when for the factor ρSg is substituted (u is the mis-placement)

$$\rho Sg + \frac{u\,q^2}{\varepsilon_0 s^2}\frac{\pi}{6}\ (+\ \rho Sg) \qquad (3.15)$$

where the term in brackets is included or excluded dependent on the orientation of the chamber. For a vertically operated chamber the extra displacement becomes

$$\delta = \frac{2u}{3}\left[\left\{\cos\left(2.35 \times 10^{-3}\sqrt{1/T}\ \ell/s\right)\right\}^{-1} - 1\right] \qquad (3.16)$$

which for most of the MWPC's considered is still small compared to u.

In concludlng this section we note that:

1) for mechanically applied tensions greater than given by eq.(3.10), the wire system is stable, and deflections are minimal
2) for an ideally constructed, and vertically operated MWPC these deflections are identically equal to zero
3) small displacements in the construction, and the effect of gravity when the chamber is operated horizontally, have a similar effect. This effect is given in eqs. (3.14) and (3.16)
4) because of the fact that eqs. (3.14) and (3.16) contain the applied tension in such a way that the deviations become smaller for larger T, and because one is not likely to construct the MWPC ideally, it is a good idea to make T as high as practicable. Table 5 is included here to assist in this choice.

3.2 Forces on the cathode planes

In the preceding section the attractive force on the wires due to the presence of the cathode planes was neglected. The reasons for this approximation are that the distances involved are much larger (greater or equal to a as opposed to s in the latter case), and also these already weaker forces are compensated for by the nearly symmetrical positions of the two cathode planes. However, on the cathode these are the only forces present, and we are therefore considering these here.

From eqs. (2.5) and (2.6) we know both the charge per unit area on the cathode, and the electric field at that position. Using the expression F = qE for the electric force on a charge q and in a field E we obtain for the force per unit area on the cathode, which we will call the electrostatic pressure p_e:

$$p_e = q^2/4\varepsilon_0 s^2 \qquad (3.17)$$

Using the relation q = 1.58×10^{-8} C/m deduced from table 3, we have calculated p_e for some different MWPC's, and give the results in table 6. As can be seen from this table these are very low pressures indeed: for the smallest pitch (s = 0.5 mm) the electrostatic pressure is the same as

that of only 3 mm of water column. In the case that the window is also used as a cathode, this pressure has to be compared with the back pressure which is needed for a flow system, or the excess pressure which occurs in a sealed chamber when it is used at a temperature different from that at which it was filled. When the chamber is used at higher pressures, these will outweigh the electrostatic pressure by several orders of magnitude (cf. 1 atmosphere is equivalent to 10^5 N/m^2).

In a flow system operated at atmospheric pressure, the backpressure is likely to be of the order of 100 N/m^2 or more, thereby making the electrostatic pressure a correction only. In a sealed system operated at atmospheric pressure, the internal pressure depends on the temperature difference between the temperature at which it is used and at which it was filled. Assuming the ambient temperature to be 23 ± 5 centigrade the differential pressure over the window ie not likely to exeed $10/300 \times 10^5$ N/m^2 = 3×10^3 N/m^3, which is again larger than the electrostatic pressure.

The effect of a uniform pressure on a foil is, unfortunately, a difficult problem to solve, and therefore we consider the following approximation. The cathode foil of length w and height ℓ, is conceived to be composed of strips δw wide (see fig.4), which respond independently to the applied pressure. The maximum depression calculated in this way will be larger than is actually the case, since neighbouring strips support each other and the strips at x = 0 and x = w are restrained to zero deflection. With increasing ratio w/ℓ, however, this effect diminishes. This assumption being made, our problem is now reduced to the one discussed in the previous section. The (uniform) force per unit

length on the strip is

$$F_a = p\delta w \tag{3.18}$$

and the restoring force

$$F_r = - T\,\delta\omega \cdot \frac{\partial^2 y}{\partial z^2} \tag{3.19}$$

where T is the force per unit length with which the foil is stretched.

The curve followed by the strip can be found by equating expressions (3.18) and (3.19) under the conditions $y(0) = y(\ell) = 0$. The result is

$$y(z) = \frac{-\,1/2\;p\;z^2}{T} + \frac{1/2\;p\;\ell z}{T} \tag{3.20}$$

The maximum depression occurs at $z = \ell/2$ and is given by

$$\delta = 1/2\;p\;\ell^2/4T \tag{3.21}$$

The elastic modulus of the material being used does not occur in this result because we have assumed that the tension, which is applied during construction, is very much larger than the extra tension induced by this small deformation. A foil of thickness t = 0.5 mm, made of beryliium, may be stretched with a force $T = 6.65 \times 10^4$ N/m (about 2/3 of its yield strength). The deflection of a 20 mm wide window will be only 10^{-3} µm per unit of pressure in that case.

If the chamber is used in a horizontal orientation, gravity must also be considered. A simple way to account for gravity is to use

$p_e + \rho t g$ instead of p in eq. (3.21), where ρ is the density of the cathode material, t its thickness and g the acceleration of gravity. 0.5 mm of Be, for example, contributes an extra 9.1 N/m^2 to the electrostatic pressure, and an extra 10^{-2} μm to the deflection, when it is stretched as above.

Although we will show in the next paragraph, that the gas amplification, and therefore the pulse height, is extremely sensitive to the anode to cathode distance, it follows from the discussion above that the electrostatic forces on the cathode are not very likely to cause problems.

3.3 Mechanical tolerances

In this paragraph the effect of the mechanical tolerances on the performance of the MWPC is discussed. Because the charge per unit length determines the gasamplification (eq. 2.9), it also determines the pulse-height, and therefore the detectability of an event. We will thus determine the effect of the mechanical tolerances on the charge on the anode wire, and convert this into an effect on the gasmultiplication. Five mis-settings will be considered: i) misplacement of an anode wire in the anode plane, ii) misplacement of the same in the perpendicular direction, iii) smoothness and parallelism of the cathode planes, iv) smoothness of the anode wires, and v) the effects of a non-uniform applied voltage, caused e.g. by contact resistances.

We will calculate these effects by a determination of the variation of eq. (2.2) as the result of a perturbation of one of the parameters a, s, d, or V_0. Although this method is only an approximation, its results are very similar to those of Erkskine [3,18] and more suitable

for our purposes because it gives an analytical expression in the parameters, mentioned before.

The misplacement of an anode wire in the anode plane is equivalent to changing the pitch s locally. The expression for dq may thus be found by differentiating eq. (2.2) with respect to s, with the result

$$\text{i)} \quad \frac{dq}{q} = \frac{c(\pi a/s - 1)}{2\pi\ \varepsilon_0} \frac{ds}{s} \tag{3.22}$$

where c is given by eq. (2.3). The misplacement in the direction perpendicular to the anode plane has no effect through the parameter a, because the dependence of eq. (2.2) on a is a result of the condition $V(x,\pm a) = 0$ (see section 1), to first order it has also no effect through the parameter s, thus the variation of q because of this disturbance is

$$\text{ii)} \quad dq/q = 0 + \mathit{0}(\Delta y)^2 \tag{3.23}$$

to first order in the displacement Δy. The smoothness and parallelism of the cathode planes will change the charge q by its dependence on the parameter a

$$\text{iii)} \quad \frac{dq}{q} = \frac{-\ c}{2\varepsilon_0 s}\, da \tag{3.24}$$

This expression reveals an important property of this effect, i.e. it is dependent on the <u>absolute</u> variation in the cathode to anode gap rather than on the <u>relative</u> variation. The variation of the diameter of the anode wire has the following effect on the charge on the anode

$$\text{iv)} \quad \frac{dq}{q} = \frac{c}{2\pi\varepsilon_0} \frac{d(d)}{d} \tag{3.25}$$

Finally, the dependence on the applied voltage is calculated very easily with the result

$$v) \quad \frac{dq}{q} = \frac{dV_o}{V_o} \tag{3.26}$$

In order to convert these expressions into equations which relate the variation in the gasamplification factor to the variation in the different parameters i) to v), we use eq. (2.9) to obtain

$$\frac{d\Lambda}{\Lambda} = \log \Lambda \cdot \frac{dq}{q} \tag{3.27}$$

Since the variation in the cases i) to v) mentioned above, are probably not interrelated, we may combine the effects as follows

$$\left(\frac{dq}{q}\right)_{total} = \left[\sum_{i=1}^{5} \left(\frac{dq}{q}\right)_i^2\right]^{1/2} \tag{3.28}$$

The largest contributions to the sum, therefore, dominate the total effect. The contributions of eqs. (3.23) and (3.24) are small compared to the rest, for (3.23) is only a second order effect, and dV_0/V_0 very much smaller than the variation in a, s, or d. An estimate of dV_0/V_0 follows from: the contact resistance is estimated to be in the order of ohms and the current per wire not greater than a few microamps. The voltage drop is then μVolts compared to the applied kVolts. The remaining three expressions (3.22), (3.24) and (3.25) are in the proportion of $(\pi a/s - 1) : (\pi a/s) : 1$, i.e. for the ratio a/s typical of the order 4, in the proportion 11:12:1. The conclusion from these observations is that the variations ds/s and da/a should be of the order of 10 times

smaller than the smoothness of the wire d(d)/d for these to have about the same effect in the total variation of q.

4. Efficiency of the MWPC

In this, very short, section we will give some data on the absorption of x-rays with an energy of 8 keV, both in the windows of the counter, and in the gas. The design parameter a depends on these figures, as it does on the errors introduced by parallax, and the increasingly more difficult problems which arise dus to the higher voltages which are needed to operate a device with a wider gap.

The data for the atomic absorption coefficients are taken from the international tables [19] table 3.2.2.A. Figure 5 represents the data on different window materials. We have chosen: the metal foils made of Be and Aℓ, synthetic materials capton (composition: $C_{22}H_{12}N_2O_5$) and mylar ($(C_{10}H_8O_4)_x$), and finally the natural product mica. In table 7 the linear absorption coefficients for these materials are assembled. All of these data are valid for radiation of wavelength $\lambda = 1.54$ Å, i.e. an energy of 8.05 keV.

Although a wide varisty, both in composition and in concentration, of quencher gas admixtures is in use at present, we present in fig.6 data on the absorption in the counter gas at a few different concentrations of quencher gas. We have used the absorption of CO_2 gas to calculate the curves in the figure, but the data may also be used for different admixtures. The reason for this is that the absorption of the quencher gas is small compared to that of the noble gas component, and therefore differences between different quencher gases have only a very small effect. The number of photons absorbed in the active volume of the

detector, finally, is given by the expression:

$$T_a = T_o \underset{\sim}{A}_{gas} \underset{\sim}{T}_{window} \qquad (4.1)$$

where T_o is the incident intensity in number of photons/sec, $\underset{\sim}{A}_{gas}$ the absorption in the gas, and $\underset{\sim}{T}_{window}$ the transmission of the window. The efficiency of the device may therefore be worked out using the data given in figs. 5 and 6.

5. Properties of the pulses

In the chamber, which is described in the preceding sections, pulses will be generated for each photon absorbed in the sensitive volume, i.e. in the gas between the cathode planes in one direction, and the two outermost anode wires in the other. These pulses, however, being of the order of a few milliVolts high, can not be processed further without being amplified. It is the aim of this section to study the interaction of the impedance at the amplifier input, possibly in parallel with that also a small capacitance, and the properties of the chamber.

The signal induced on the anode wire is partly due to the electrons which are moving towards the anode wire, partly to the positive ions on their way to the cathode. To determine their relative weight we recall that the signal induced is proportional to the decrease in energy of the moving charges i.e. to the "voltage-drop" they experienced. The electrons do, between two successive ionizing collisions, gain not much more than the ionization potential, i.e. 10 to 20 eV. Half of the electrons are produced so near to the wire that they do not cause another stage in the avalanche, i.e. traversed only a few tens of Volts. The positive

ions, however, never gain so much energy as is necessary to cause ionizing collisions, because most of their energy is lost in elastic processes at much lower energies. Therefore, the positive ions traverse a much greater potential difference, even at times as short as 100 nsec, and account for the greater part of the signal. This follows from the following estimate.

The drift velocity of the ions v is direct proportional to the electric fieldstrength:

$$\vec{v} = u \vec{E} \qquad (5.1)$$

where the constant of proportionality is called the mobility u. Near the wire we may use the expression

$$E = \frac{q}{2\pi\varepsilon_0} \frac{1}{r} \qquad (5.2)$$

found from table 2. Using the following numbers: $\varepsilon_0 = 8.85 \times 10^{-12}$ F/m $q = 1.58 \times 10^{-8}$ C/m, and $u = 10^{-4}$ m^2/Vs, we calculate that the ions traverse a distance of 0.1 mm from the wire in about 100 nsec, i.e. a potential difference of about 200 to 400 V. Therefore the electron part of the signal is about 10 times weaker than the ion part. The difference becomes larger if we take longer periods of time into account. In what follows we shall therefore neglect the contribtion of the electrons to the signal.

As already mentioned above, the avalanche produces most of the electrons and therefore most of the ions very near to the anode wire. There

fore we will describe the event in the following way. A pulse from the MWPC is thought to be very near to a pulse obtained by moving a charge Q from the wire to the cathode. The charge Q is the charge of the number of primary electron-ion pairs N multiplied by the gasamplification:

$$Q = NAe \tag{5.3}$$

N may be estimated by dividing the energy of the incident radiation by the energy needed for an ionization. The pulse induced on the anode wire is then given by Wilkinson's formula [20]

$$Q(t) = NAe(q/4\pi\varepsilon_o V_o)\, \ell n\{(t+t_o)/t_o\} \tag{5.4}$$

t_o in this formula is given by

$$t_o = \frac{2\varepsilon_o s^2}{q\,\pi\,u}\, \ell n\{\cosh(\pi d/2s)\} \tag{5.5}$$

t_o is a characteristic time constant of the detector, and it seems therefore useful to see which of the parameters of the chamber affect this quantity. In order to do this more easily than is permitted by eq. (5.5), we expand the $\ell n\{\cosh(\pi d/2s)\}$ in a Taylor series around the point $d/s = 0$. This ratio will be small in any design which we consider. The result of this expansion reads:

$$t_o = \varepsilon_o \pi d^2/4qu + \ldots \tag{5.6}$$

Taking into account the conclusion drawn from table 3, i.e. q is a constant, one observes that the time-development of the pulses from a MWPC

depend only on the mobility of the positive ions, (i.e. the gas) and is proportional to the square of the wire diameter. In particular it is independent of the pitch and the gap between anode and cathode. It is straightforward to show that eq. (5.6) is just equal to the inverse of the constant which is used by Erskine [18] who arrives at his formulae via a different route.

In fig.7 a schematic drawing is given which represents the system we want to study here. The resistor R represents the input impedance of the amplifier, C_{par} is a parasitic capacitance parallel to it, and aw is the anode wire. The potential at point A is given by the following equations. Let $Q_1(t)$ be the actual charge on the anode wire in excess of the charge q per unit length which is already present in the absence of a pulse. This charge is the difference of Q(t) as is given in eq. (5.4) and that which is drained through the resistance R:

$$Q_1(t) = Q(t) - \int_0^t i(t')\, dt' \tag{5.7}$$

Furthermore, Ohm's law applies:

$$\underset{\sim}{V}_0(t) = i(t)\, R \tag{5.8}$$

and, in the case $C_{par} = 0$:

$$\underset{\sim}{V}_0(t) = Q_1(t)/c\ell \tag{5.9}$$

where c is the capacitance per unit length of the wire, and ℓ its length. From eqs.(5.7) through (5.9) we derive the following differential

equation:

$$\frac{dv_0(t)}{dt} = \frac{dQ(t)}{dt}\frac{1}{c\ell} - \frac{v_0(t)}{Rc\ell} \qquad (5.10)$$

This equation may be solved, with a series as a result. In order to present the solution in a simple way, we represent the exponential-integral function Ei(x) in a series as usual:

$$Ei(x) = \ln(x) + x + \frac{1}{2.2!}x^2 + \ldots + \frac{1}{n.n!}x^n + \ldots \qquad (5.11)$$

The solution to eq.(5.10) then becomes:

$$v_0(t) = \frac{ANe}{4\pi\varepsilon_0 \ell} \exp\{-(t+t_0)/Rc\ell\}\left\{Ei\left(\frac{t+t_0}{Rc\ell}\right) - Ei\left(\frac{t_0}{Rc\ell}\right)\right\} \qquad (5.12)$$

The current flowing through the amplifier may also be derived from this equation, by application of Ohm's law (5.8). Because we made use of Wilkinson's formula eq.(5.4) in the derivation of eq.(5.12), this latter expression is valid only for $t < 100\text{-}200$ nsec, and will converge within this region for a reasonable number of terms.

In fig.8 the time evolution of the voltage peak is shown for a few values of the input impedance R of the preamplifier. One observes clearly the decreasing pulse height and pulse duration with decreasing value of R. For fast counting purposes, therefore, a low value of the input impedance is favourable, but it becomes increasingly more difficult to detect the pulse in the noise, which is always present. To obtain a short but detectable pulse we choose that value of R which maximises the

power transferred to the amplifier. To show that this maximum exists it suffices to point out that i) if $R = 0$ a signal current flows, but no potential difference is present, so no work is done, ii) if $R = \infty$ the reverse is the case, and again no work is done, and iii) for a finite $R \neq 0$ both a signal current and a voltage are present, therefore at least one maximum will be present.

The maximum of the power pulse as a function of the input impedance of the amplifier is given in fig.9 for three different counters. In order to facilitate the comparison of the three different curves, the abscissa of this graph is not the impedance R directly but the ratio of the timeconstants $Rc\ell$ and t_0. It appears that the maximum occurs at $Rc\ell \approx 3t_0$ for each of the three chambers. This relation has been checked by performing similar calculations for 60 different chambers with parameters in the regions: a ranging from 1 to 10 mm, s from 0.5 to 2 mm and d from 10 to 20 μm.

Figure 10 shows the results of the peak heights obtained in these calculations. If plotted vs $1/R_{opt}$, where R_{opt} is the optimum impedance of the amplifier, a straight line is obtained. Using the relation $R_{opt}c\ell = 3t_0$ we conclude from this figure that, in order to obtain the best pulses, a MWPC should have a large capacitance c and a small intrinsic timeconstant t_0.

The effect of the parasitic capacitance C_{par}, finally, does not alter many of the conclusions discussed in the preceding paragraphs. It is easy to show that eq.(5.12) changes to:

$$v_0(t) = \frac{ANe}{4\pi\varepsilon_0}\,\frac{c}{c\ell+C_{par}}\,\exp\{-(t+t_0)/R(c\ell+C_{par})\}$$
$$\times\ \{Ei((t+t_0)/R(c\ell+C_{par})) - Ei(t_0/R(c\ell+C_{par}))\} \qquad (5.13)$$

The effect of these changes is that the signal becomes smaller for increasing C_{par}, and that the optimum in the input impedance in this case occurs at $R(c\ell + C_{par}) \approx 3t_0$.

In this section the interaction between the multi-wire chamber and the amplifier to which it is connected, is studied. It is argued that the best detectable pulses are obtained by choosing the input impedance of the amplifier R such that the maximum power is transferred from MWPC to amplifier. It is shown that this maximum exists, and occurs at $R_{opt} \approx 3t_0/(c\ell+C_{par})$. Finaily, the highest pulses are obained from detectors with higher capacitance and smaller timeconstant t_0.

6. Resolution

In this section, we will discuss the effects of the absorption process on the resolution of a MWPC. The resolution of this device is given by the pitch s in the present application, i.e. detection of low energy x-rays. However, the absorption processes in the gas set a lower limit to the resolution. In order to investigate this we start with a description of the absorption in the gas. Hereafter we will calculate the response of a detector on a primary absorption of a photon at x = 0. From this the lower resolution limit will be derived.

The interaction of electromagnetic radiation with matter may follow different mechanisms, depending on the energy of the photons. The most important processes are photoelectric conversion, Compton scattering and

absorption, Raleigh scattering and pair-production. Clearly, the latter process cannot occur at the low energies of interest here. Of the remaining processes the photoelectric conversion is by far the most probable. For the noble gases Ar and Xe, for instance, the absorption coefficient as a result of photoelectric effect is 10-100 m^2/kg at a photon energy near 10 keV, whereas Compton scattering, the second most probable effect, contributes only 0.01-0.1 m^2/kg [2] at that energy. We will therefore consider only the photoelectric effect.

The reaction products after the absorption of a photon are an electron, which is knocked out of the atom, and a positively charged and excited ion. The electron is stopped in the gas producing further electron-ion pairs in less violent reactions. The excited ion loses its excess energy either by emitting a fluorescent x-ray, or by the Auger effect. In this latter process a rearrangement of the electrons in the cloud occurs, accompanied by the emission of a second electron, which carries the excess energy. The Auger effect is the most likely to occur in atoms with a low atomic number, and its probability increases with decreasing exitation energy. In the former of the two mechanisms an x-ray is produced with an energy just below an absorption edge and consequently having a relatively long range. This photon may escape the active volume of the detector, or initiate a second reaction. The fluorescence yield of this second reaction (see table 8) is very much lower than for the first, so we may neglect further primary reactions.

In order to evaluate the effects of these events on the resolution of the detector, the dimensions of the cloud of electron-ion pairs produced by the photo-electron or the Auger electron have to be determined together with the probability distribution of the absorption of the fluo-

rescent x-rays within the detector volume. The former data can be found in ref.[21], fig.2, from which the data in table 9 are inferred. From this table follows that the best resolution possible in a detector operated at atmospheric pressure and at ambient temperature is about 200 μm when filled with argon and about half this number when filled with xenon. This resolution becomes better with increasing operating pressure.

The effect of the fluorescent photons on the spatial resolution of the chamber is found by calculating the number of fluorescent photons absorbed in pixcel 0, ± 1, ± 2, ... when one incident photon is absorbed in pixcel 0. The probability of absorption in an infinitesimal small volume dv with (polar) coordinates (r,θ,ϕ), is proportional to the flux incident on that volume. Assuming a uniform angular distribution for the emission of the fluorescent quantum, we may obtain this probability distribution by using the normalisation condition:

$$\int_{r=0}^{\infty} \int_{\theta=o}^{\pi} \int_{\phi=0}^{2\pi} r^2 \sin\theta \, P(r) \, dr \, d\theta \, d\phi = \omega \qquad (6.1)$$

where P(r) is the probability of absorption of a fluorescent photon a distance r apart from a single primary event. From this condition, and the proportionality to the incident flux, the following expression for P(r) is obtained:

$$P(r) = \frac{\omega\mu^3}{8\pi} \exp(-\mu r) \qquad (6.2)$$

where μ is the linear absorption coefficient. The number of absorption events in a pixcel of a linear counter may then be expressed as follows:

$$I(n) = \int_{\theta=0}^{\theta_{max}} \int_{r=r_{min}}^{r_{max}} \int_{\phi=0}^{2\pi} P(r) \, r^2 \sin\theta \, dr \, d\theta \, d\phi \qquad (6.3)$$

where n is the pixcel-number, θ_{max} the largest polar angle of a volume-element within the active volume of the pixcel, and r_{min} and r_{max} the minimum and maximum distance from the origin of an element of the pixcel. θ_{max} is calculated by

$$\theta_{max} = \tan^{-1}(a/ns) \qquad (6.4)$$

and r_{min} and r_{max}:

$$r_{min} = (n - \tfrac{1}{2})s/\cos\theta$$
$$r_{max} = (n + \tfrac{1}{2})s/\cos\theta \qquad (6.5)$$

The integral (6.3) is calculated with the approximation $\theta_{max} = \pi/2$. For large values of n, where r_{min} is large and therefore the integrand P(r) very small, this is a good approximation for all values of a. For small n, this approximation is valid for large values of a (compared to s). Figure 11 shows the results for a few values of s and μ. A faint halo is observed to appear around the central peak, positioned at the pixcel in which the absorption of the incident ray occurred. The halo becomes stronger and less extended for increasing μ and s, and therefore affects the resolution in these cases more.

7. Conclusion

In this report information has been assembled from the literature, augmented at several places with a new analysis of the data available,

which might prove useful in the design of a multiwire, linear detector of low energy x-rays e.g. for a small angle scattering experiment. Special attention has been given to the effects of making the pitch of the anode wires narrower than the value of 1 mm which is readily available at present. From this analysis it follows that, although the mechanical requirements are more severe for a s = 0.5 mm detector, its construction seems to be feasible theoretically. The criteria for mechanical and electrical stability have been deduced, and the relative importance of some mechanical tolerances assessed. Finally it has been shown that an optimum input impedance of the (pre-)amplifier exists, and its value is calculated as a function of the chamber parameters.

Summary

In this report information is assembled on the mechanical and electrical properties of multiwire proportional chambers, useful in the design of a particular detector. In order to obtain reasonably simple formulae very many approximations had to be made. Many of these have been checked against exact results, where available. The most important conclusions from the different sections will be given here as a further aid.

i) From section 5, and fig.10 in particular, it was concluded that, in order to obtain the best pulses R_{opt} should be as small as practicable i.e. t_0 small and c large. t_0 is proportional to the wire-diameter squared, therefore d should be small.

ii) Mechanical stability requires the highest possible tension on the anode wires (see section 3.1). This requirement calls for thicker wires.

iii) Electrical stability is obtained by manufacturing the detector to very tight tolerances. These tolerances are proportional to c (section 3.3). For this reason c should be chosen as small as possible, but this is again at variance with i).

iv) A wide operating range of applied voltages is obtained by using the thickest possible anode wires, but the lowest operational voltage is found in detectors with thin wires.

v) The experimental requirements may impose some extra restrictions (e.g. the gap width should be at least a certain value for efficiency reasons, or at most another to obtain good resolution).

vi) The distance between the anode and the cathode plane, and the pitch of the wires are the most important dimensions, and should be manufactured to very tight tolerances (see section 3.3).

Clearly, one has to find a compromise to these conflicting requirements. This report provides the following to help in this process. From table 3 we learn that detectors built in the decade 1972-1982, for widely varying purposes, and with widely varying dimensions use almost the same value of q (= 1.58 10^{-8} C/m). Secondly, explicit relations are providsd to calculate the effect of the electrical and mechanical properties. For instance section 3.3 gives the relation between electrical properties and mechanical tolerances whereas section 3.1 gives the contribution to the mechanical tolerances of the electrostatic forces.

Acknowledgement

It is a pleasure to mention here the very pleasant discussions I have had with J. Worgan during the time that this report was prepared.

References

[1] G. Charpak, R. Bouclier, T. Bressani, J. Favier, and Č. Zupančič; Nucl. Instr. and Meth. 62 (1968) 235.

[2] F. Sauli; CERN-report CERN 77-09 (1977).

[3] G.A. Erskine; Nucl. Instr. and Meth. 105 (1972) 565.

[4] S.P. Beingessner; and L. Bird; Nucl. Instr. and Meth. 172 (1980) 613.

[5] J.E. Bateman, priv. comm.

[6] J.E. Bateman, J.F. Conolly, E.C. Sawyer, and R. Stephenson; Nucl. Instr. and Meth. 196 (1982) 515.

[7] J.E. Bateman, J.F. Conolly, R. Stephenson, and G.J. Tappern; Nucl. Instr. and Meth. 190 (1981) 385.

[8] J.E. Bateman and J.F. Conolly; Nucl. Instr. and Meth. 173 (1980) 525.

[9] G. Charpak and F. Sauli; Nucl. Instr. and Meth. 113 (1973) 381.

[10] G. Charpak, H.G. Fisher, C.R. Gruhn, A. Minten, F. Sauli, and G. Plch; Nucl. Instr. and Meth. 99 (1972) 279.

[11] A.R. Faruqi, IEEE trans. nucl. sci; NS30 (1983) 358.

[12] A.R. Faruqi and C.C. Bond; Nucl. Instr. and Meth. 201 (1982) 125.

[13] J. Hendrix, H. Fuerst, B. Hartfiel, and D. Dainton; Nucl. Instr. and Meth. 201 (1982) 139.

[14] S. Kitamoto; Nucl. Instr. and Meth. 198 (1982) 595.

[15] M.R. Sims, H.D. Thomas, and M.J.L. Turner; IEEE trans. nucl. sci. NS28 (1981) 825.

[16] A.C. Thompson; Nucl. Instr. and Meth. 195 (1982) 303.

[17] S. Kitamoto; Nucl. Instr. and Meth. 203 (1982) 613.

[18] G.A. Erskine; Nucl. Instr. and Meth. 198 (1982) 325.

[19] International Tables for X-ray Crystallography Vol.III; C.H. Macgillavry and G.D. Rieck, ed. (1968) Kynoch Press.

[20] G. Charpak; Ann. Rev. Nucl. Sci. 20 (1970) 195.

[21] G. Charpak, F. Sauli, and R. Kahn; Nucl. Instr. and Meth. 152 (1978) 185.

List of symbols

a	cathode to anode distance	(m)
A	gas amplification factor	
$\underset{\sim}{A}$	absorption	
c	capacitance per unit length	(F/m)
C	capacitance	(F)
d	diameter of anode wire	(m)
d_c	diameter of cathode wire	(m)
e	electronic charge e = 1.60 × 10^{-19} C	(C)
$\vec{E}$	electric field strength	(V/m)
E_0	electric field strength at anode surface	(V/m)
F	force or force per unit length	(N or N/m)
g	acceleration of gravity g = 9.8 m/s^2	(m/s^2)
$\vec{i}$	unit vector in x-direction	
I	(transmitted) intensity	(photons/sec)
I_0	(primary) intensity	(photons/sec)
$\vec{j}$	unit vector in y-direction	
$\vec{k}$	unit vector in z-direction	
l	length of anode-wires	(m)
m	mass	(kg)
M	Youngs modules	(N/m^2)
n	number n = 0, ± 1, ± 2, ...	
N	number of primary electron-ion pairs	
p	pressure	(N/m^2)
p_e	elecrostatic pressure	(N/m^2)
P	power	(W)
q	charge per unit length	(C/m)
Q	charge	(C)
r	radius (polar-coordinate)	(m)

$\vec{R}$	position-vector measured from anode wire	
R	input impedance	(Ω)
s	pitch of anode wires	(m)
s_c	pitch of cathode wires	(m)
S	area of cross section	(m^2)
t	thickness	(m)
T	tensile force	(N for wires N/m for foils)
$\underset{\sim}{T}$	transmission	
u	mobility of ions	(m^2/Vs)
v	drift velocity	(m/s)
$\underset{\sim}{V}_0$	signal voltage	(V)
V	electric potential	(V)
V_0	applied high tension	(V)
w	width of window	(m)
x	cartesian coordinate	
y	cartesian coordinate	
z	cartesian coordinate	
δ	deflection	(m)
ε_0	permitivity of vacuum ε_0 = 8.85 pF/m	(F/m)
θ	polar angle	
λ	wavelength	(m)
λ_a	mean free path for absorption	(m)
μ	absorption coefficient	(m^{-1})
σ	charge per unit area	(C/m^2)
φ	azimuthal angle	
ω	fluorescence yield	

Table 1. Deviations from uniformity a distance y from the anode plane (in units of the pitch s). E_x and E_y are the calculated field strengths in units of $q/2\varepsilon_0 s$.

y	E_x	$E_y - 1$
0.5	9.4×10^{-2}	9.0×10^{-2}
1	3.7×10^{-3}	3.7×10^{-3}
1.5	1.6×10^{-4}	1.6×10^{-4}
2	7.0×10^{-6}	7.0×10^{-6}
2.5	3.0×10^{-7}	3.0×10^{-7}
3	1.3×10^{-8}	1.3×10^{-8}

Table 2. The three important field regions in a MWPC with flat cathodes. n in the bottom line takes the values n = 0, ± 1, ± 2, ...

Description of field region	Boundaries in space	Expression for $\vec{E}$
high, radial field	$\left\|\vec{R}\right\| \lesssim 0.1s$	$\vec{E}(\vec{R}) = (q/2\pi\varepsilon_0).\vec{R}/\left\|\vec{R}\right\|^2$
uniform field region	any x, z	$\vec{E}(x,y,z) = (q/2\varepsilon_0 s).\vec{j}$
low field region	any z, y ≈ 0 x ≈ (n + 1/2)s	$\vec{E}(x,y,z) \approx 0$

Table 3.

Gas mixtures are denoted by numbers: (1) 30% isobutane; (2) 21% isobutane + 4% metylal; (3) 24.5% isobutane + 0.5% freon; (4) 30% CO_2; (5) 10% CH_4; (6) 7% CH_4. Note the relative constancy of E_0 and q. The values for q scatter around $q = 1.58 \times 10^{-8}$ C/m with a standard deviation of 0.37×10^{-8} C/m.

a (mm)	s (mm)	d (μm)	V_0 (kV)	E_0 (10^7 V/m)	q (10^{-8} C/m)	p (10^5 N/m^2)	gas	ref.
6	0.5	10	8	3.95	1.10	1	Xe+(1)	[5]
6	1	20	6.8	3.15	1.75	1	Xe+(1)	[6]
6	1	10	6.1	5.47	1.52	1	Xe+(1)	[7]
8	2	20	5.8	3.62	2.01	1	Xe+(1)	[8]
8	3	30	3.5	1.97	1.64	1	Ar+(2)	[9]
6.6	2	20	5.7	4.12	2.29	1	Ar+(3)	[10]
8	2	20	5.7	3.56	1.98	1	Ar+(3)	[10]
5	1	10	3.75	3.91	1.09	1	Xe+(4)	[11]
5	1	10	4	4.17	1.16	1	Xe+(1)	[12]
3	1	10				3	Xe	[13]
3.7	0.58	20	7	3.14	1.74	1	Ar+(5)	[14]
5	2	15	3.55	4.08	1.70	2	Xe+(5)	[15]
10	2	20	4.2	2.19	1.22	1	Ar+(6)	[16]
0.7	0.58	20	1.4	2.33	1.29	1	Ar+(5)	[17]

Table 4. Electrostatic forces on anode wires in chambers with different pitches, operated at a charge of 1.58×10^{-8} C/m, compared with gravity forces on wires of different thicknesses. The density of tungsten ($\rho = 19.3 \times 10^3$ kg/m^3) was used.

s(mm)	F(N/m) per μm deflection	d (μm)	F_g (N/m)
0.5	8.88×10^{-5}	5	0.37×10^{-5}
1	2.22×10^{-5}	10	1.48×10^{-5}
2	5.56×10^{-6}	20	5.92×10^{-5}

Table 5. Maximum permissible tensile force for tungsten wire of different diameter. The numbers given, are calculated using the elastic modulus $M = 3.4 \times 10^{11}$ N/m^2, and a maximum permissible elongation of $d\ell/\ell = 6 \times 10^{-3}$.

d (μm)	T (N)
5	0.040
10	0.160
15	0.361
20	0.641
30	1.442

Table 6. Electrostatic pressure on cathode planes in MWPC's with different values of s, the pitch of the anode wires. The chambers are assumed to be operated at a charge per unit length of anode wire equal to $q = 1.58 \times 10^{-8}$ C/m.

s(mm)	$P_e(N/m^2)$
0.5	28.2
1.0	7.1
2.0	1.8
3.0	0.8
4.0	0.4
5.0	0.3

Table 7. Linear absorption coefficients of different window materials. The transmission of a foil with thickness t is calculated by $\underset{\sim}{T} = \exp(-\mu t)$. Data are valid for 8 keV radiation.

material	μ (m^{-1})
Al	1.31×10^4
Be	277.5
Capton	869
Mylar	935
Mica	9.43×10^4

Table 8. Fluorescence yield ω of the two most important detector gases. Note the large decrease with decreasing excitation energy. Data are taken from ref.21.

Gas	ω_K(%)	ω_L(%)
Ar	12	0.02
Xe	88	11

Table 9. Energy and range of reaction products after the absorption of an 8 keV x-ray in a detector. The range of a photon may be defined as $\lambda_a = 1/\mu$.

	Ar	Xe
Photoelectrons:		
E (keV)	4.8	3.6
range (μm)	200	70
Auger electrons:		
E (keV)	$\lesssim$ 2.9	$\lesssim$ 4.1
range (μm)	100	70
Fluorescent x-ray:		
E (keV)	~ 3.1	~ 4.3
μ (m^{-1})	25.6	200
λ_a (mm)	39	5

Figure captions

Fig.1 Typical arrangement of the electrodes in a MWPC.

Fig.2 Electrostatic forces on two parallel and charged wires. The total force per unit length dℓ is calculated using the expression for the Coulomb force and integrating over the angle α.

Fig.3 Electrostatic forces on a MWPC structure.

Fig.4 Dimensions and orientation of the cathode foil. All sides are built in, and stretched with a force T per unit length. One of the strips, discussed in the main text, is shown.

Fig.5 The transmission for different window materials as a function of thickness. Linear absorption coefficients given in table 7 have been used.

Fig.6 Absorption of 8 keV radiation in a MWPC as a function of depth. The top scale indicates the associated value of the design-parameter a. Gases are indicated by numbers; 1: Xe, 2: 90% Xe + 10% quencher, 3: 70% Xe + 30% quencher, 4: Ar, 5: 90%Ar + 10% quencher, and 6: 70% Ar + 30% quencher. The total pressure in the chamber is 10^5 N/m^2 (atmospheric), type of quencher used: CO_2.

Fig.7 Schematic drawing of a detector wire connected to a (pre-) amplifier.

Fig.8 Voltage signals from a MWPC with parameters a = 5 mm, s = 1 mm, d = 10 μm. The pulses are drawn for two different values of the input impedance R of the amplifier, and scaled to unit gas amplification A.

Fig.9 The maximum value of the signal pulse. This graph displays the maximum of the power-pulse as a function of the ratio of the RC-time and the intrinsic time constant t_0. Curve 1 is for a chamber with the parameters a = 5 mm, s = 1 mm, d = 10 μm: curve 2: a = 5 mm, s = 0.5 mm, d = 10 μm and 3: a = 5 mm, s = 2 mm, d = 20 μm. Each chamber is operated at a charge on anode wire of q = 1.58 × 10^{-8} C/m, and have anode wires of 1 m long. Pulses are scaled to unit gas amplification A.

Fig.10 Maximum value of the signal pulse for 60 different detectors, each terminated with the optimum impedance R_{opt}. The detectors ordered according to this quantity. All points are on the the straigt line displayed.

Fig.11 Number of counts I(n) in pixcel n when one incident photon is absorbed in pixcel 0. The halo is due to capture of fluorescent x-rays produced in ths primary reaction. The value used for the fluorescence yield is ω = 0.12 which is the case for Xe. The linear absorption coefficient μ = 1000 m^{-1} applies for a detector filled to a pressure of 5 atmosphsre, and μ = 200 m^{-1} for atmospheric pressure.

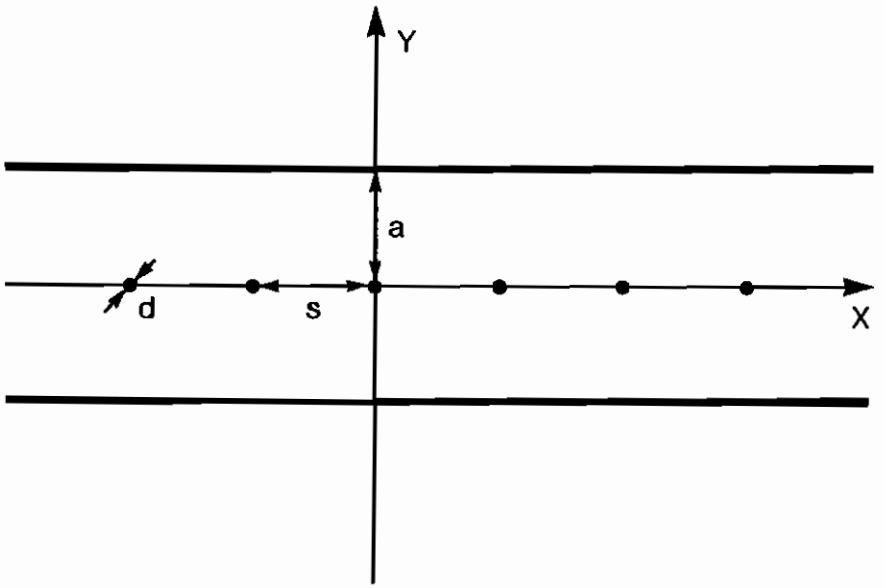

Fig.1

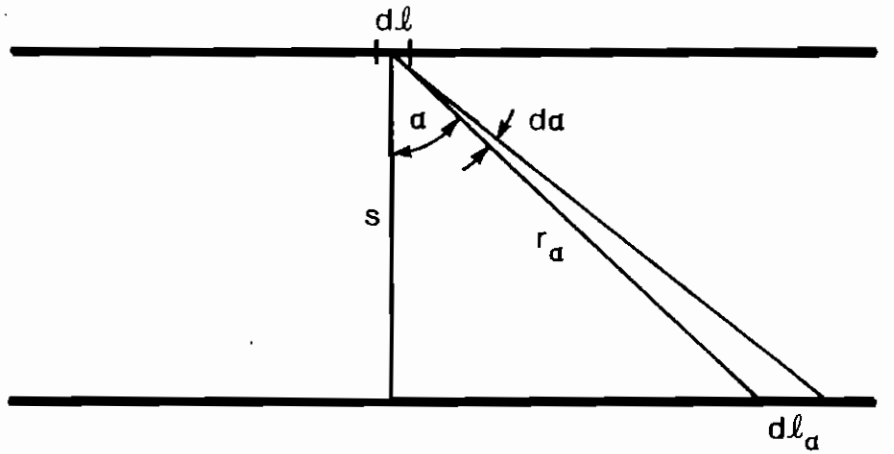

Fig.2

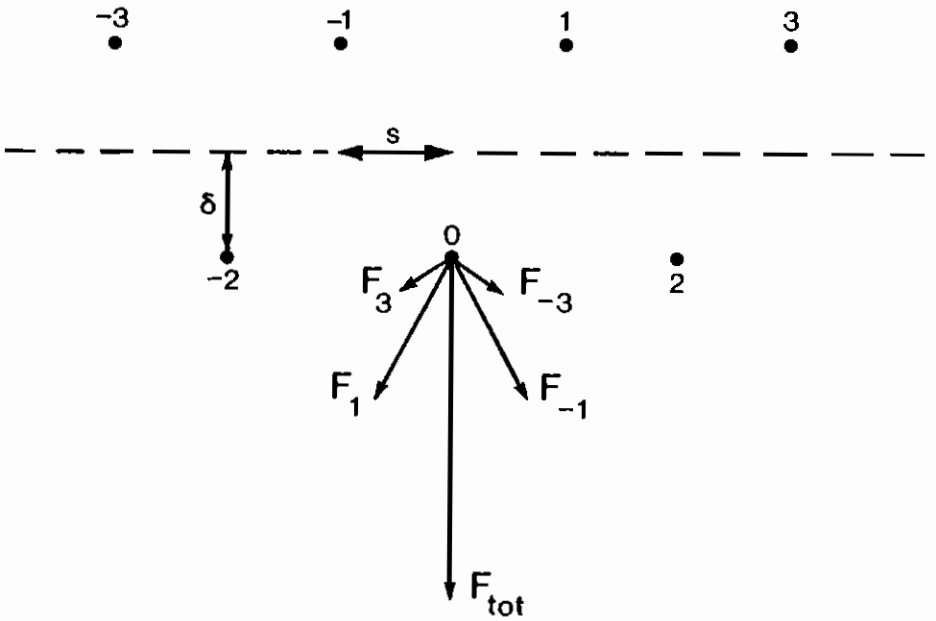

Fig. 3

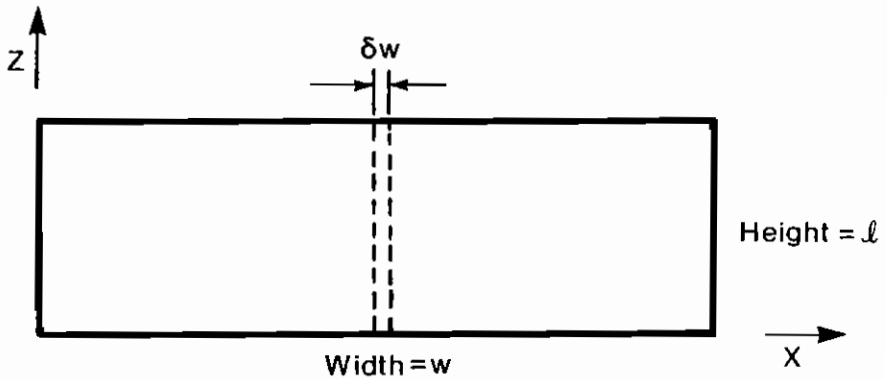

Fig. 4

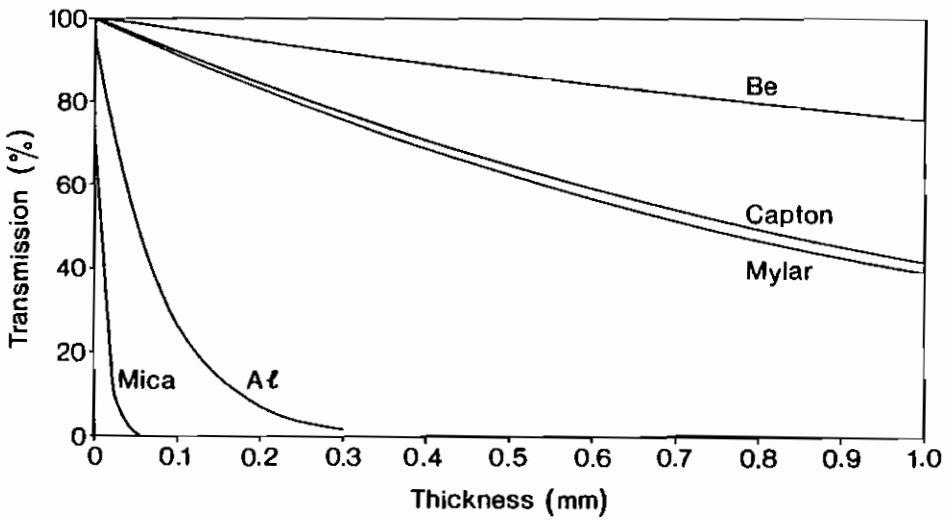
Transmission (%)
100
80
60
40
20
0
0
0.1
0.2
0.3
0.4
0.5
0.6
0.7
0.8
0.9
1.0
Thickness (mm)
Be
Capton
Mylar
Mica
Aℓ

Fig.5

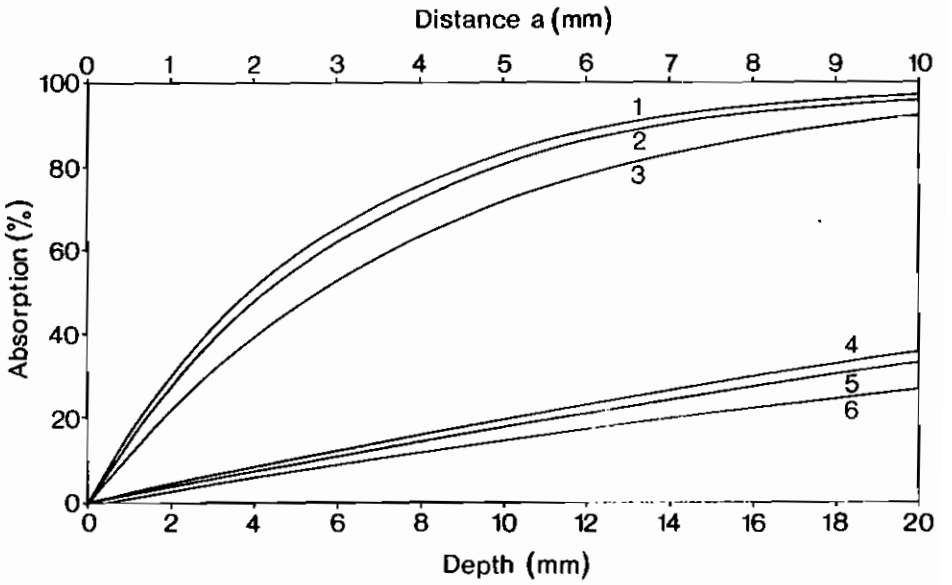
Distance a (mm)
0
1
2
3
4
5
6
7
8
9
10
Absorption (%)
100
80
60
40
20
0
0
2
4
6
8
10
12
14
16
18
20
Depth (mm)
1
2
3
4
5
6

Fig. 6

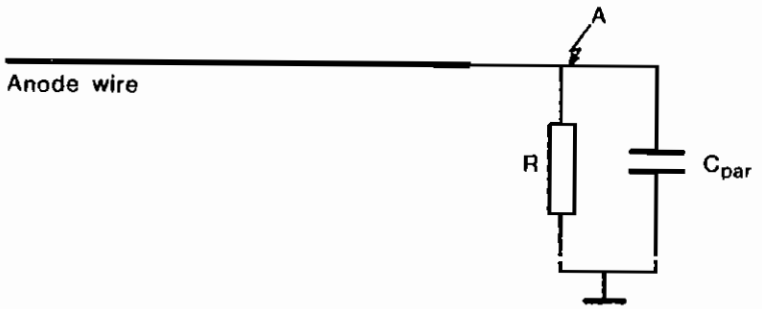
A
Anode wire
R
C_{par}

Fig. 7

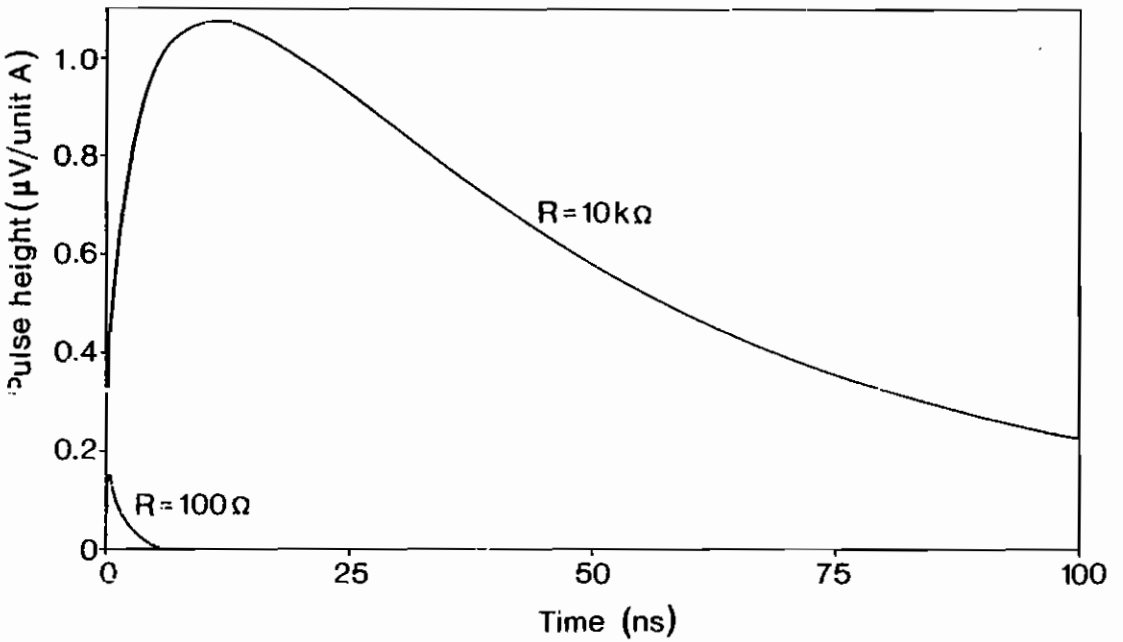
Pulse height (μV/unit A)
1.0
0.8
0.6
0.4
0.2
0
R = 10 kΩ
R = 100 Ω
0
25
50
75
100
Time (ns)

Fig. 8

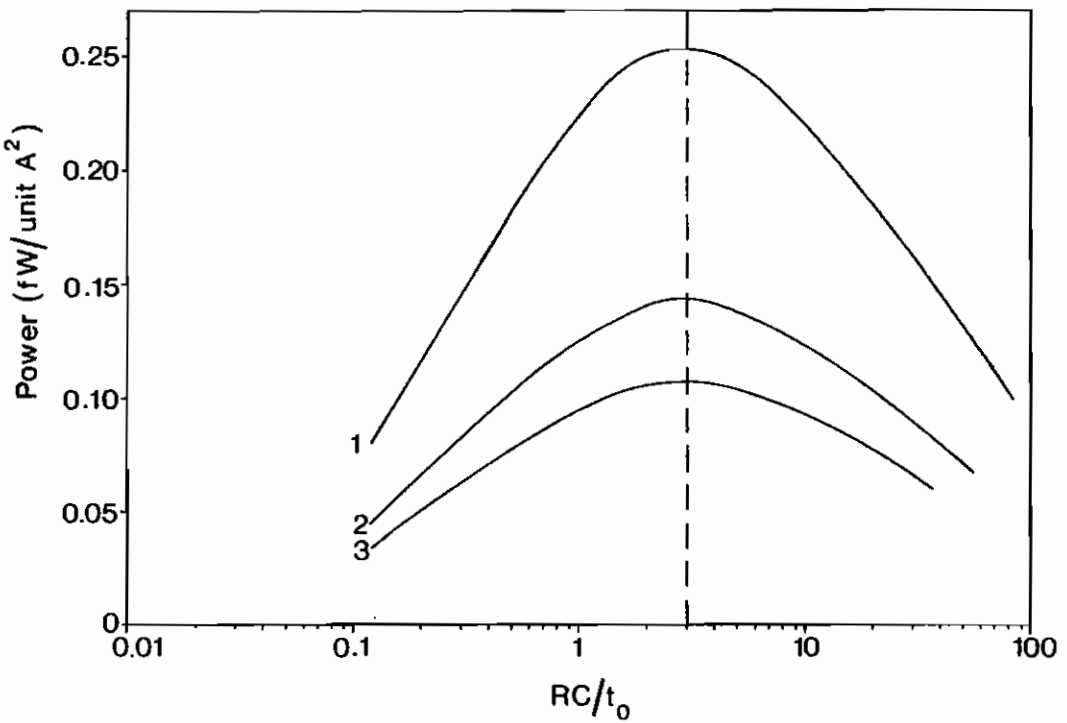
Power (fW/unit A²)
0.25
0.20
0.15
0.10
0.05
0
0.01
0.1
1
10
100
RC/t₀
1
2
3

Fig. 9

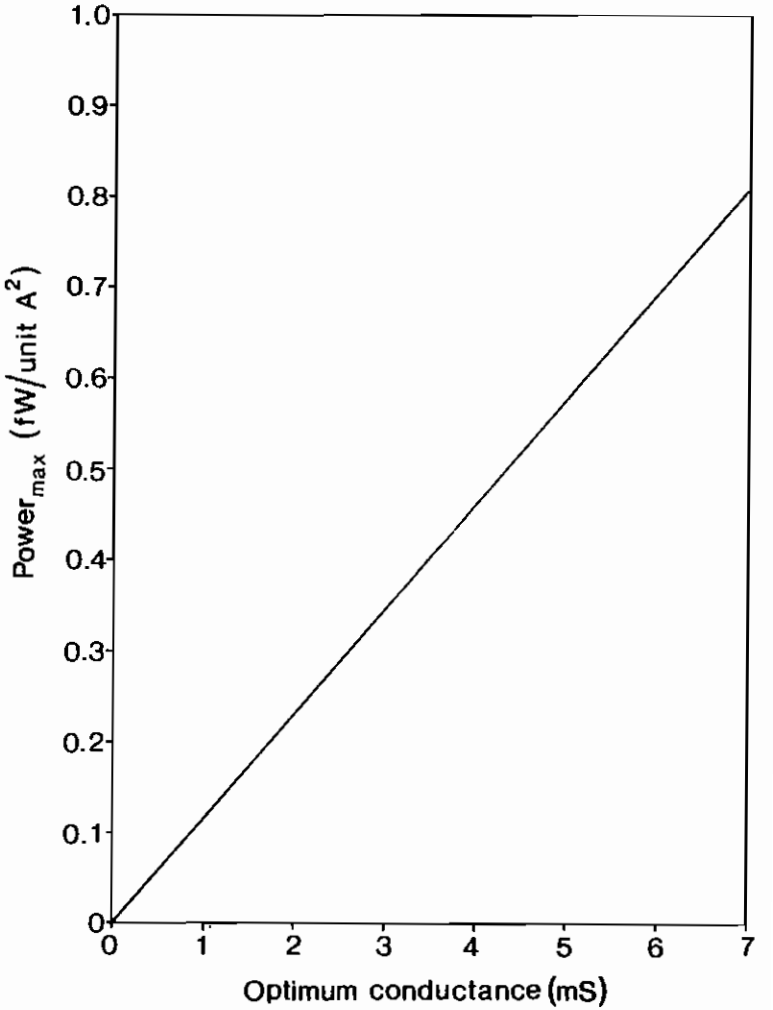
Power_max (fW/unit A²)
1.0
0.9
0.8
0.7
0.6
0.5
0.4
0.3
0.2
0.1
0
0
1
2
3
4
5
6
7
Optimum conductance (mS)

Fig. 10

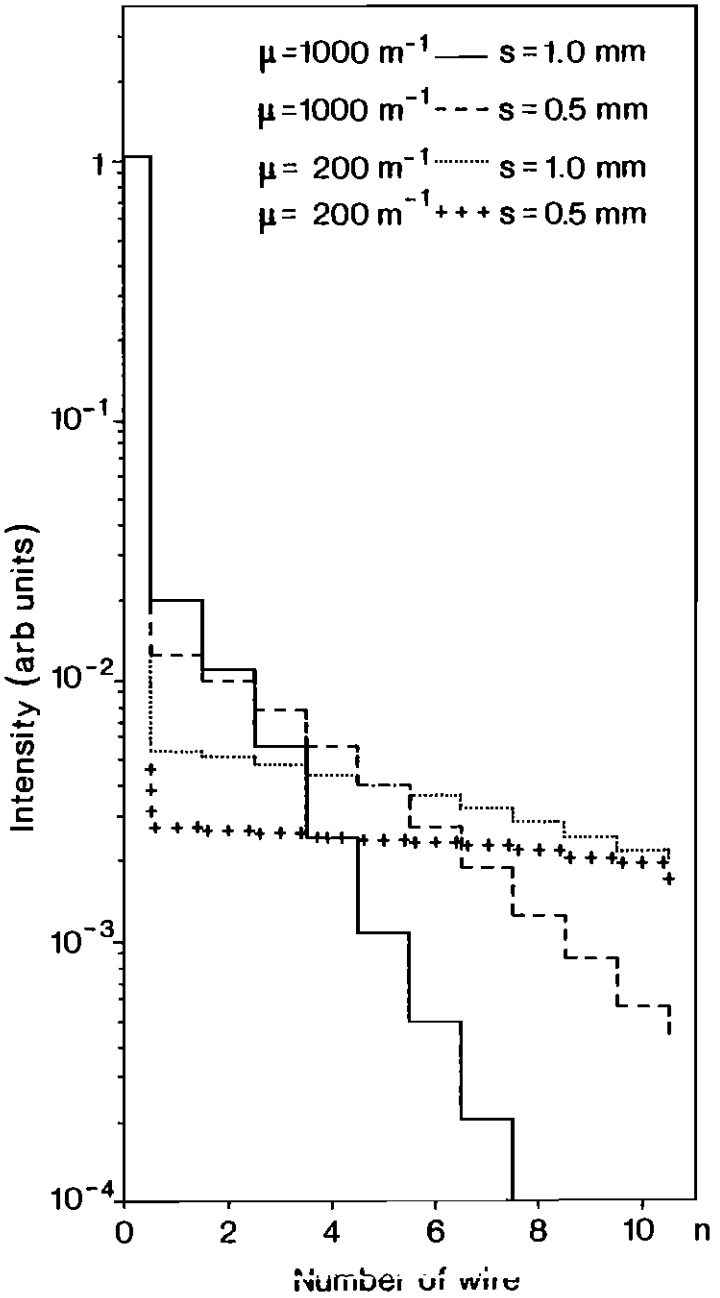
μ=1000 m^{-1} —— s=1.0 mm
μ=1000 m^{-1} - - - s=0.5 mm
μ= 200 m^{-1} ····· s=1.0 mm
μ= 200 m^{-1} + + + s=0.5 mm
Intensity (arb units)
1
10^{-1}
10^{-2}
10^{-3}
10^{-4}
0
2
4
6
8
10
n
Number of wire

Fig. 11